Supplement of Atmos. Meas. Tech., 13, 5739–5761, 2020
https://doi.org/10.5194/amt-13-5739-2020-supplement


Atmospheric Measurement Techniques
Open Access
EGU

*Supplement of*

# Measurement of $NO_x$ and $NO_y$ with a thermal dissociation cavity ring-down spectrometer (TD-CRDS): instrument characterisation and first deployment

**Nils Friedrich et al.**

*Correspondence to:* John N. Crowley (john.crowley@mpic.de)

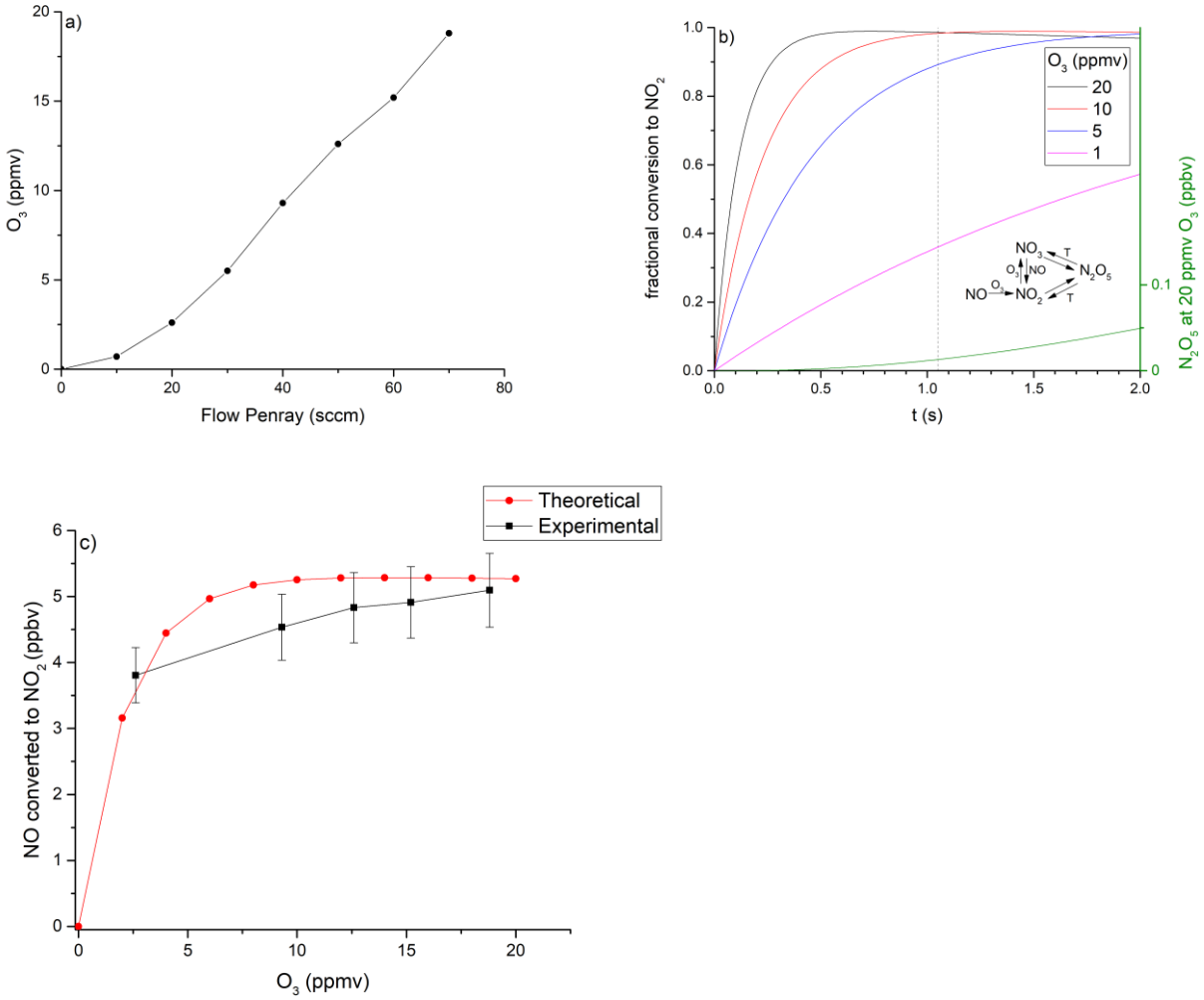


**Figure S1:** Optimisation of NO to $NO_2$ conversion via the addition of $O_3$. *a)* Ozone generated by passing synthetic air over the Pen-Ray lamp as a function of the flow rate. *b)* Numerical simulation of the fractional NO conversion as a function of reaction time and a chemical scheme showing reactions included in the model. High concentrations of $O_3$ can lead to the formation of significant amounts of $N_2O_5$ (50 pptv at 20 ppmv $O_3$ and 2 s reaction time). *c)* Conversion of 5.3 ppbv NO to $NO_2$ as a function of $O_3$ in 1.05 s reaction time. Both laboratory results and predictions of a numerical simulation are shown. Quantitative conversion is achieved for $O_3$ concentrations above 15 ppmv. The error bars indicate total overall uncertainty.

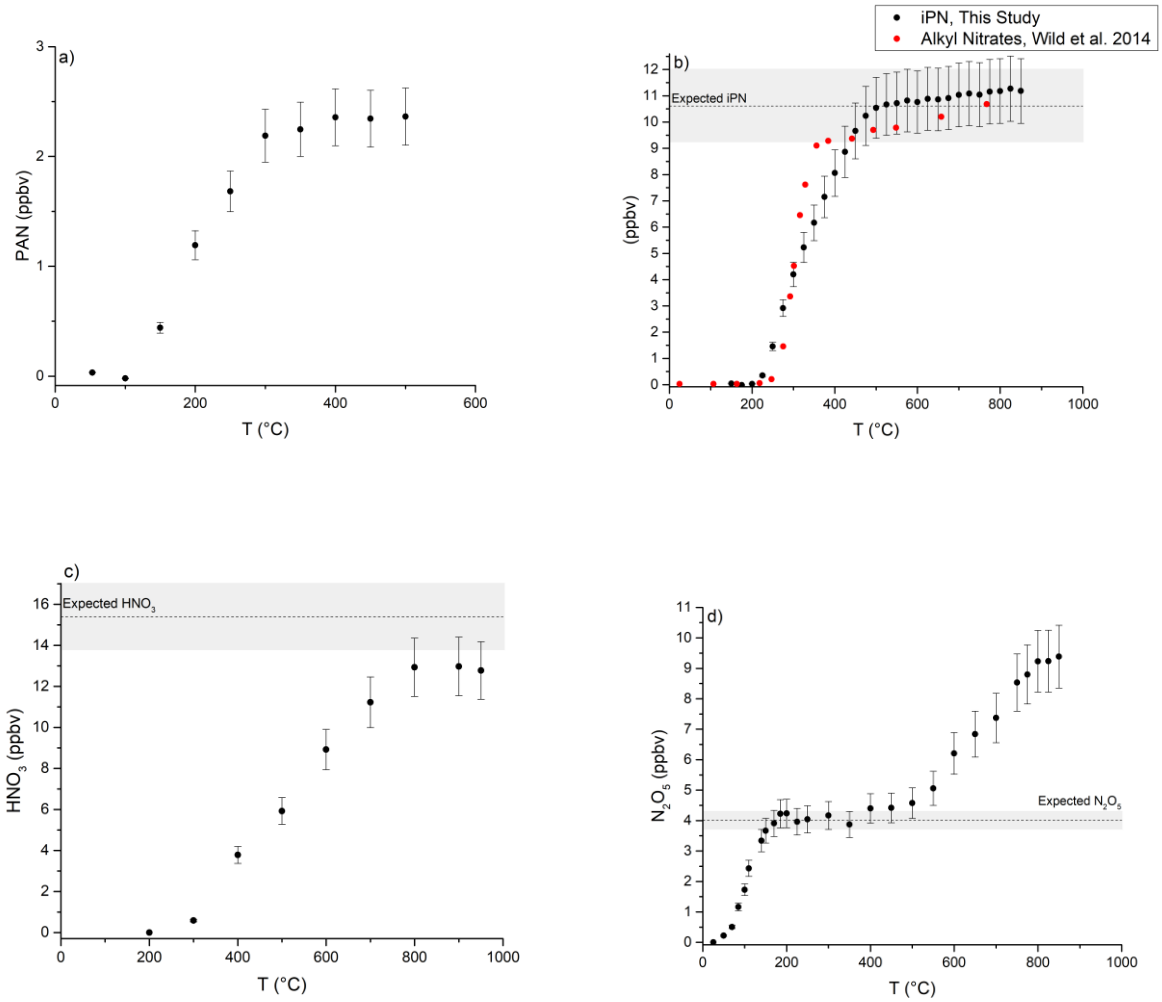


**Figure S2:** Absolute thermograms of PAN *(a)*, iPN *(b)*, $HNO_3$ *(c)*, and $N_2O_5$ *(d)*. Error bars represent the measurement uncertainty (see Sect. 2.2). Shaded areas show the estimated uncertainty ranges for the expected iPN and $HNO_3$ concentrations, based on errors during sample preparation and gas stream dilution. Within combined uncertainties we observe quantitative conversion of PAN, iPN, 2x $N_2O_5$ and $HNO_3$ to $NO_2$ at the TD-CRDS set temperature of 850 °C. *(b)* also includes data points for an alkyl nitrates mixtures from Wild et al. (2014), to illustrate the continuous increases in signal above 400 °C.

*Wild, R. J., Edwards, P. M., Dube, W. P., Baumann, K., Edgerton, E. S., Quinn, P. K., Roberts, J. M., Rollins, A. W., Veres, P. R., Warneke, C., Williams, E. J., Yuan, B., and Brown, S. S.: A measurement of total reactive nitrogen, NOy, together with $NO_2$, NO, and $O_3$ via cavity ring-down spectroscopy, Env. Sci. Tech., 48, 9609-9615, doi:doi:10.1021/es501896w, 2014*

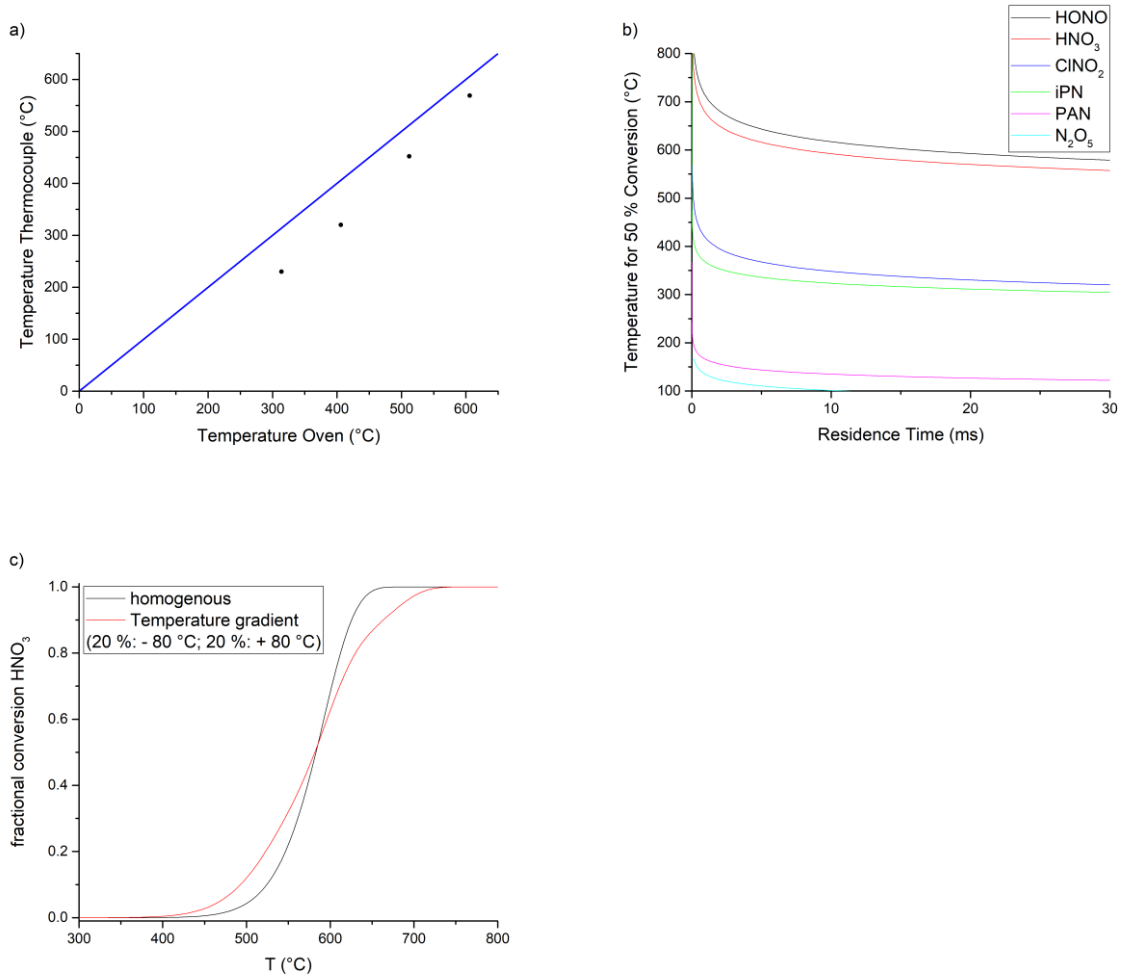


**Figure S3:** a) Plot of temperature from the internal reading of the TD-oven and a thermocouple located in the gas stream. The blue line shows a 1:1 correlation. b) Calculated threshold temperature for 50% conversion of $N_2O_5$, PAN, iPN, $ClNO_2$, $HNO_3$ and HONO to $NO_x$ relative to the residence time in the heated inlet and based on kinetic parameters of their thermal dissociation (see Sect. 3.1.8). For HNO3, the threshold temperature increases by 40 °C when the residence time decreases from 30 to 10 ms. c) Impact of temperature gradients inside the TD-inlet on the shape of the calculated $HNO_3$ thermogram. The width of the thermogram increases by ca. 100 °C.

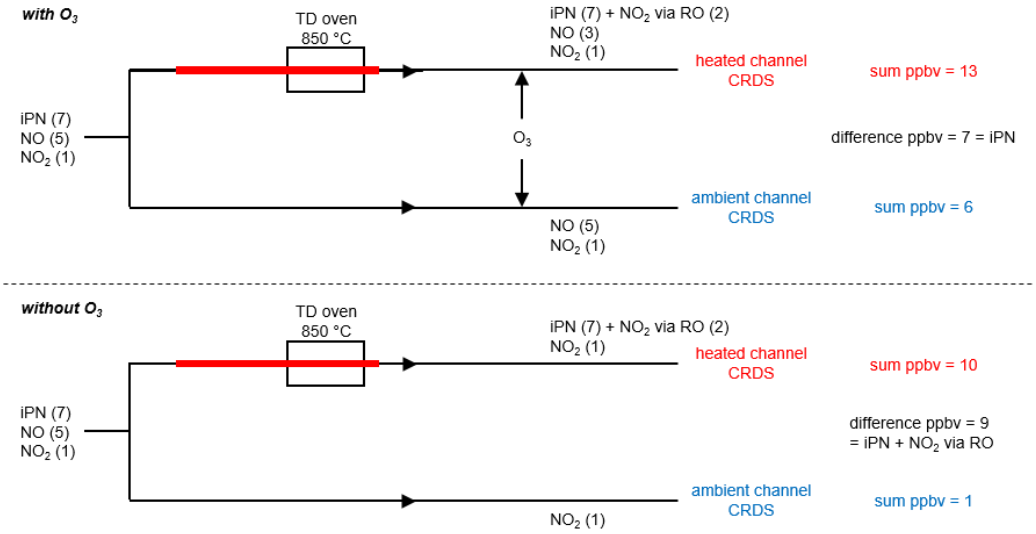


**Figure S4:** Graphical representation of the bias caused by $RO_2$ + NO reactions in detecting iPN. In both cases an initial mixing ratio of 7 ppbv iPN is present, along with 5 ppbv NO and 1 ppbv $NO_2$. When passed through the oven the iPN is converted to 7 ppbv $NO_2$ and (in this scenario) 2 ppbv of NO are converted to $NO_2$ via reaction with $HO_2$. In total 13 ppbv of $NO_2$ are detected in the cavity sampling via the oven. In the cavity at ambient temperature 6 ppbv of $NO_2$ are detected so that a (correct) iPN mixing ratio of 7 ppbv is derived. In the lower part of the figure, the same initial conditions apply, but $O_3$ is not added. The conversion of 2 ppbv NO to $NO_2$ occurs as above, so that 10 ppbv $NO_2$ are detected when sampling from the oven. The $NO_2$ mixing ratio in the cavity sampling at ambient is 1 ppbv, resulting in a derived (incorrect) $NO_2$ iPN mixing ratio of 9 ppbv.

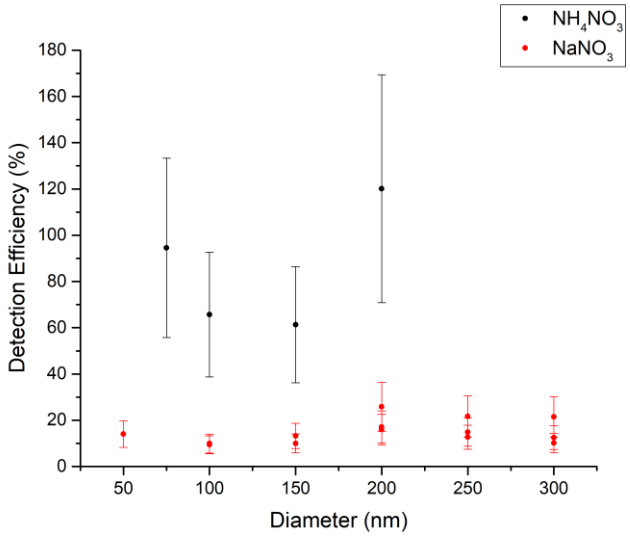


**Figure S5:** Detection efficiencies of $NH_4NO_3$ and $NaNO_3$ in the TD-CRDS, as a function of particle diameter. The CPC measured particle numbers were converted to mixing ratios and compared to the TD-CRDS. Errors imminent for this method are explained in Sect. 3.1.7. The particle conversion to $NO_2$ is clearly more efficient for $NH_4NO_3$, in direct comparison to $NaNO_3$.

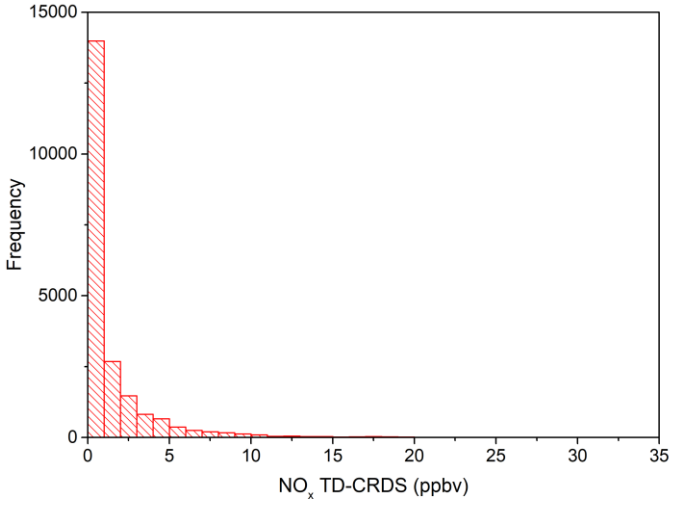


**Figure S6:** Histogram of the AQABA TD-CRDS $NO_x$ mixing ratios shown in Fig. 10a). 92 % of the $NO_x$ data points were at mixing ratios below 5 ppbv.

**Table S1:** Reactions included in the numerical simulations used to generate Fig. S1.

| **Reaction** | **Rate coefficients (**Burkholder et al. (2015) |
|---|---|
| $NO_2 + O_3 \rightarrow NO_3 + O_2$ | 1.2E-13*exp(-2450/T) |
| $NO + NO_3 \rightarrow NO_2 + NO_2$ | 1.5E-11*exp(170/T) |
| $NO + O_3 \rightarrow NO_2 + O_2$ | 3.0E-12 *exp(-1500/T) |
| $N_2O_5 \rightarrow NO_3 + NO_2$ | (((2.0E-30*(T/300)^-4.4)*M/(1+((2.0E-30*(T/300)^-4.4)*M/(1.4E-12*(T/300)^-0.7))))*0.6^((1+(LOG10((2.0E-30*(T/300)^-4.4)*M/(1.4E-12*(T/300)^-0.7)))^2)^-1))/(3.0E-27*exp(10990/T)) |
| $NO_2 + NO_3 \rightarrow N_2O_5$ | ((2.0E-30*(T/300)^-4.4)*M/(1+((2.0E-30*(T/300)^-4.4)*M/(1.4E-12*(T/300)^-0.7))))*0.6^((1+(LOG10((2.0E-30*(T/300)^-4.4)*M/(1.4E-12*(T/300)^-0.7)))^2)^-1) |

M = molecular density in molecule $cm^{-3}$, T = temperature in K.

*Burkholder, J. B., Sander, S. P., Abbatt, J., Barker, J. R., Huie, R. E., Kolb, C. E., Kurylo, M. J., Orkin, V. L., Wilmouth, D. M., and Wine, P. H.: Chemical Kinetics and Photochemical Data for Use in Atmospheric Studies, Evaluation No. 18," JPL Publication 15-10, Jet Propulsion Laboratory, Pasadena, http://jpldataeval.jpl.nasa.gov., 2015.*

**Table S2:** Denuder characterisation

| **$NO_y$ species** | **RH (%)** | **Reference mixing ratio (pptv) = $I_0 \pm \Delta I_0$** | **Mixing ratio with denuder (pptv) = $I \pm \Delta I$** | **Removal efficiency (%) = $(R \pm \Delta R) \times 100$** |
|---|---|---|---|---|
| NO | 0 | 37036 ± 261 | 0 ± 43 | 100.0 ± 1.0 |
| | 14 | | 62 ± 46 | 99.8 ± 1.0 |
| | 28 | | 832 ± 94 | 97.8 ± 1.0 |
| | 42 | | 7832 ± 60 | 78.9 ± 0.9 |
| | 55 | | 10391 ± 65 | 71.9 ± 0.9 |
| | 68 | | 12575 ± 45 | 66.0 ± 0.9 |
| | 81 | | 13758 ± 51 | 62.9 ± 0.8 |
| | 97 | | 14220 ± 74 | 61.6 ± 0.9 |
| iPN | 0 | 20181 ± 247 | 0 ± 22 | 100.0 ± 1.0 |
| | 14 | | -98 ± 91 | 100.5 ± 1.0 |
| | 27 | | -65 ± 58 | 100.3 ± 1.0 |
| | 41 | | 355 ± 49 | 98.2 ± 0.9 |
| | 55 | | 303 ± 41 | 98.5 ± 0.9 |
| | 68 | | 537 ± 47 | 97.3 ± 0.9 |
| | 81 | | 907 ± 46 | 95.5 ± 0.8 |
| | 95 | | 1043 ± 33 | 94.8 ± 0.9 |
| $HNO_3$ | 0 | 8224 ± 214 | 35 ± 58 | 99.6 ± 2.7 |
| | 68 | 9104 ± 173 | 247 ± 50 | 97.3 ± 3.7 |
| $NO_2$ | 0 | 24259 ± 211 | 54 ± 45 | 99.8 ± 1.3 |
| | 65 | 24164 ± 225 | 448 ± 40 | 98.1 ± 1.2 |
| PAN | 0 | 7575 ± 93 | 58 ± 130 | 99.2 ± 2.4 |
| $N_2O_5$ | 0 | 4179 ± 230 | 5 ± 48 | 99.9 ± 7.8 |
| HONO | 46 | 10000 ± 61 | 1521 ± 47 | 84.8 ± 0.9 |
| $ClNO_2$ | 60 | 2068 ± 103 | 521 ± 141 | 74.8 ± 9.2 |

Mixing ratios (reference determined in heated inlet with bypassed denuder), standard deviations (1σ) during the averaging intervals and derived denuder removal efficiencies of various $NO_y$ species, as a function of RH and as presented graphically in Fig. 6. $R = (I_0 - I) / I_o$. $\Delta R$ was determined by error propagation.